Design and Experimental Implementation of an Electromagnetic Engine Valve Drive

T. A. Parlikar, *Student Member, IEEE*, W. S. Chang, *Member, IEEE*, Y. H. Qiu, *Student Member, IEEE*, M. D. Seeman, *Student Member, IEEE*, D. J. Perreault, *Member, IEEE*, J. G. Kassakian, *Fellow, IEEE*, and T. A. Keim, *Member, IEEE*

***Abstract*—In conventional internal combustion engines, engine valve displacements are fixed relative to crankshaft position. If these valves were actuated as a variable function of crankshaft angle, significant improvements in fuel economy could be achieved. To this end, a new type of electromagnetic valve drive system (EMVD) for internal combustion engines was more recently proposed. This EMVD incorporates a disk cam with a very desirable nonlinear profile which that functions as a nonlinear mechanical transformer. Modeling and simulation results showed significant advantages of this EMVD over previously designed electromagnetic engine valve drives. In this articles, we describe an experimental implementation of the proposed EMVD, which was developed to confirm these benefits. The EMVD apparatus was designed, constructed, and integrated into a computer-controlled experimental test stand. The experimental results confirm the benefits of using a nonlinear mechanical transformer in a motordriven engine-valve spring system, as seen in the small average power consumption and low valve seating velocity. In addition, a valve transition time sufficient for 6000-rpm engine operation was achieved. The results also suggest ways to improve the EMVD apparatus in the future.**

***Index Terms*—Actuator, cam, camless engine, variable valve actuation, variable valve timing (VVT).**

I. Introduction

EVEN AFTER a century of development, the internal combustion (IC) engine continues to evolve. Modern engines are more efficient than their predecessors because they produce more power per unit mass or volume and are cleaner. Many features of IC engines have been reengineered. In more recent years, variable valve actuation has been one of the more promising technological improvements [1]–[3]. In some respects, the electromechanical valve drive (EMVD) represents the ultimate in variable valve actuation.

Manuscript received June 17, 2004; revised December 5, 2004. Recommended by Technical Editor M. Mavroidis. This work was supported by the Sheila and Emanuel Landsman Fund at the Massachusetts Institute of Technology.

T. A. Parlikar, Y. H. Qiu, D. J. Perreault, J. G. Kassakian, and T. A. Keim are the Laboratory for Electromagnetic and Electronic System, Massachusetts Institute of Technology, Cambridge, MA 02139 USA (e-mail: parlikar@mit.edu; yiqiu@mit.edu; djperrea@mit.edu; jgk@mit.edu; tkeim@mit.edu).

W. S Chang was with the Laboratory for Electromagnetic and Electrnic System, Massachusetts Institute of Technology, Cambridge, MA 02139 USA. He is now with Varian Semiconductor, Gloucester, MA USA (e-mail: wschang@alum.mit.edu).

M. D. Seeman was with Laboratory for Electromagnetic and Electrnic System, Massachusetts Institute of Technology, Cambridge, MA 02139 USA. He is now with the Department of Electrical Engineering and Computer Sciences, University of California, Berkeley, CA 94720 USA (e-mail: mseeman@eecs.berkeley.edu).

Digital Object Identifier 10.1109/TMECH.2005.856221

In conventional IC engines, valve displacement is a fixed function of crankshaft position. The valves are actuated by cams located on a belt- or chain-driven camshaft, and the shape of these cams is determined by considering a tradeoff between engine speed, power, and torque requirements, as well as vehicle fuel consumption. This optimization results in an engine that is highly efficient only at certain speeds [4]. If instead the engine valves are actuated as a variable function of crankshaft angle, engine load, and other parameters, significant improvements in fuel economy can be achieved [5].

IC engines in which both the duration (how long each valve is opened or closed) and the phase (when each valve is opened or closed) of the valves can be controlled are said to have variable valve timing (VVT) [6]. In some VVT systems, it is also possible to control the lift (the displacement from the closed to open position) of the valve. With variable valve timing alone, a 10% improvement in fuel economy can be achieved [5].

We begin this article by giving some background on VVT systems and discussing the variable valve actuation systems described in the literature and then focus on the proposed EMVD, including details on the modeling and control of the EMVD, its implementation in the laboratory, and the experimental results. In Section II, we discuss VVT systems and variable valve actuation systems described in the literature. The proposed EMVD is discussed in Sections III and IV. In Section V, we offer some design and control considerations for the EMVD. We describe the EMVD experimental apparatus in Section VI. Finally, controller design and experimental results are described in Section VII.

II. Variable Valve Timing Systems

An IC engine valve's kinematics profiles (e.g., valve position versus time, valve speed versus time) are of fixed shape and are timed relative to the engine crankshaft position. With an electromagnetically driven VVT system, one can independently control the phase and duration of the engine valve profiles, as well as carry out variable engine displacement, where certain cylinders in the engine may be deactivated. In these systems, the valves can be held in the open or closed positions for a variable time called the holding time. They can also be commanded to transition from fully open to fully closed positions or vice versa (the valve stroke). They make this transition at a time that is well suited to the engine's instantaneous operation.

In effect, VVT systems would replace the current camshaft-driven valve actuation systems. To this end, VVT systems must have some of the same features as conventional valve actuation systems, while allowing the additional flexibility mentioned

previously to be feasible [7]. First, the average mechanical power loss at the engine associated with driving a typical 16-valve, 2.0-L, four-cylinder engine at 6000-rpm engine speed and wide-open throttle is 2–3 kW [7]. Thus, for any VVT system to be competitive, the effective mechanical power loss must be on this order of magnitude. Second, the seating velocity, the velocity at which an engine valve engages its seat, of the typical IC engine valve is small: less than 3 cm/s at 600-rpm engine speed and less than 30 cm/s at 6000-rpm engine speed [6]. To prevent excessive wear of engine valves and limit acoustic noise, any VVT system should allow for the "soft" landing of the valve; that is, the valve must engage its seat at or below these velocities. Third, any VVT system must efficiently allow for a valve transition time (the time in which the valve moves from 5% of the stroke to 95% of the stroke) on the order of 3–4 ms or faster. These fast transition times allow the engine to operate at speeds of 6000 rpm or higher. Fourth, from a control systems perspective, any VVT system must be able to operate as intended in the presence of varying gas forces. Gas forces are particularly significant for engine exhaust valves. Finally, a "lash-adjustment" device that takes the thermal expansion of the engine valves into account must also be incorporated into the VVT. In addition to these features, to be a viable alternative to conventional IC engine valve trains, VVT systems must be economically and technically feasible. In this respect, component cost, durability, and packaging must also be taken into consideration.

There are many types of variable valve actuation systems, each classified according to the way it operates. Some of these systems are not electromechanically actuated and may not achieve variable valve timing as defined previously, however, they still demonstrate better-optimized engine performances than in conventional IC engines.

The most popular mechanically actuated valve systems are the variable cam phasing (VCP) and cam profile switching (CPS) types. In VCP, the cam phase is shifted with respect to the crankshaft. Except for the shift in phase, the valve lift versus crank angle profile is totally unaltered. Among other features, this characteristic means that a change in valve opening angle causes an equal change in valve closing angle. VCP systems are commonly used in double overhead camshaft (DOHC) engines, in which case one actuator can control either the intake or exhaust valve phase. Control of both types of valves requires two actuators.

In CPS systems, the effect is the same as shifting from one cam to another. The lift, duration, and phase of the second cam can all be different from the first cam, but the operational choice is between one fixed valve displacement profile and another. Both VCP and CPS are popular, owing to their design simplicity, and many automotive companies have already used these approaches in production models [8]–[10]. Other approaches used in variable valve actuation include electropneumatic [11] and electrohydraulic [4] valve actuators, which are described extensively in the literature.

The most viable electromechanically actuated valve drive system to date is the normal-force actuator-based electromechanical valve drive (NFEMVD) [1]. Prototype NFEMVD systems have been proposed by several companies in the automotive industry, the first being proposed and patented by FEV Moterentechnik [1], [12]. Other companies that have worked on this technology include BMW [13], [14], GM [15]–[17], Renault [18], Siemens [4], [19], and Aura [20].

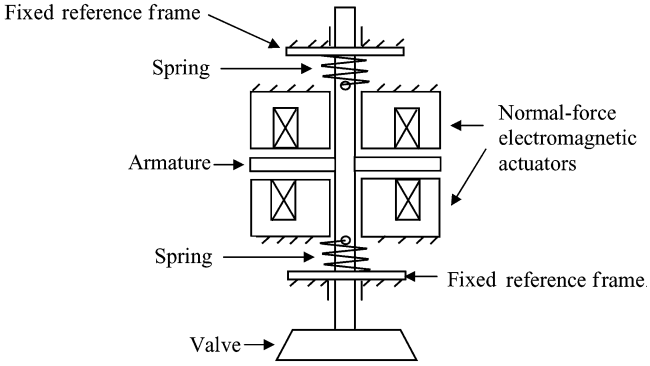

Fig. 1. Normal-force actuated electromechanical valve drive.

In the NFEMVD, two solenoids are used to control a resonant valve-spring system: one to hold the valve open, and one to hold the valve closed. Each electromagnet exerts a unidirectional normal-force, and thus, the system employs two normal-force actuators. Fig. 1 shows such a normal-force actuated valve drive system.

An engine valve is coupled to two springs in the resonant valve-spring system in Fig. 1. The equilibrium position for this mass-spring system is in the middle of the valve stroke. Such a system has an inherent natural frequency (ω_n), mass (M), effective spring constant (k), and damping ratio (ζ). If there were no damping, an initial displacement of the valve in the direction of either spring would result in sustained oscillations of the valve at the system's natural frequency. The valve can be held at either end of the stroke by the application of a force that does no work. If the valve is released from rest at one end of the stroke, it arrives at the other end of the stroke with zero velocity. In the ideal frictionless case, considering only the valve-spring system dynamics, the electric motor only has to be able to hold the valve at either end of its stroke. In reality, additional work is required to reject the gas force disturbance and to compensate for friction.

The benefit of using springs in the NFEMVD is that they, ideally, allow lossless transitions of the valve from one end of the stroke to the other. Once an initial amount of energy is injected into the system by compressing one of the springs, that energy is converted to kinetic energy and then transferred from that spring to the other spring continuously. The inertial (reactive) power for accelerating and decelerating the valve mass at the required rates is thus stored internally, and does not need to pass through an external source.

In the NFEMVD, the force exerted by each electromagnetic actuator is proportional to the square of the current input, but decreases as a function of the air gap between the actuator and the armature [21], [22]. Hence, these actuators have a nonuniform force constant. For a fixed level of current, each solenoid can exert a large force when the valve is very close to the solenoid, but small forces when the valve is a short distance away from the solenoid. For example, when the valve is at either end of the stroke, the relevant solenoid can produce a large force with

a relatively small current. Thus, there is low holding current at both ends of the stroke. However, when the valve is at the lower end of its stroke, a large upward force requires a very large current in the upward-acting solenoid.

Because of the actuators used in the NFEMVD, there are substantial control challenges to achieving soft landing with normal-force actuators [21]–[23]. First, because the normal-force actuators are unidirectional, it is impossible to decelerate the valve as it approaches an end of its stroke—to arrive exactly at the end of the stroke with exactly zero velocity (defined as perfect soft landing), the receiving-end actuator must do exactly as much work as was done against friction and gas force over the entire transition. If the actuator does not do this much work, the valve will stop before the end of the stroke and will be driven away again by the spring. If the actuator does any more than the exactly correct work, the valve arrives at the end of the stroke with nonzero velocity and impacts the valve seat.

A second control challenge is that the electromagnetic actuators have a nonuniform force constant [22], making it difficult to apply enough force to the valve when it is close to the equilibrium point of the system. Thus, it is difficult to counteract the effects of the gas force disturbance on the system.

To control valve seating velocity and reject gas force disturbances on the engine valves, one must take these design constraints into account when designing a controller. (see [21], [23]–[25] and the references therein) have shown that, in the absence of gas forces, soft landing can be achieved using a carefully designed nonlinear controller. However, it is not yet known how the inclusion of gas forces will impact this controller.

A possible solution to the control challenges in the normal-force actuated valve-spring system is to attempt to use a bidirectional shear force actuator to control the resonant valve-spring system. An example of such an actuator is a rotary electric motor. Such actuators have uniform force constants and can exert bidirectional forces. Henry *et al*. [16], [17] showed that with a motor-actuated resonant valve-spring system (MAEMVD) and an active controller, the effect of gas force is reduced. However, there are problems with this VVT system. First, the holding current is very high because the spring forces at the ends of the stroke are large. Second, the required driving current for the controller to reject the gas force disturbances is also large. Thus, the corresponding power loss of this VVT system, even at low effective engine speeds ($\leq$2000 rpm), is too large to be economically feasible [7].

In the next section, we describe the proposed EMVD, which attempts to eliminate the control challenges of both the NFEMVD and the MAEMVD drive, while continuing to use their most desirable feature: the resonant valve-spring system.

III. The Proposed EMVD

The proposed EMVD comprises an electric motor (similar to the MAEMVD) that is coupled to a resonant valve-spring system via a slotted cam, which acts as a nonlinear mechanical transformer (NTF). As in the NFEMVD, there are two fixed reference frames at either end of the two springs (later referred to as the top and bottom plates). As the motor rotates, the roller moves within the slotted cam, allowing the valve to move vertically. As the valve moves, it compresses one spring and extends the other.

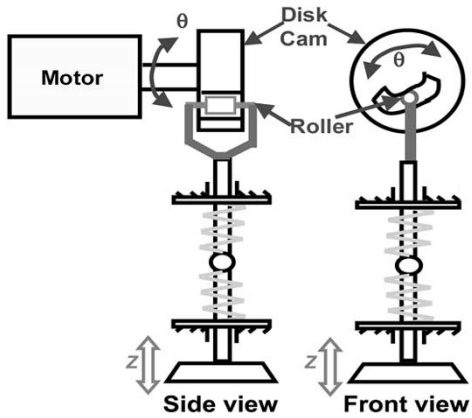

Fig. 2. Schematic of the proposed EMVD in which the nonlinear mechanical transformer is implemented as a disk cam with a nonlinear relation prescribed in its slot.

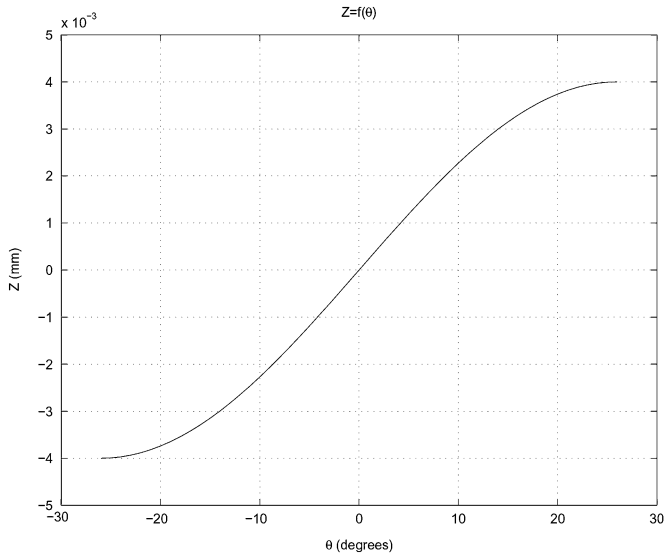

Fig. 3. Desirable transfer characteristic for the nonlinear mechanical transformer. The slope of this profile is the gear ratio of the EMVD when viewed from the θ domain.

Fig. 2 shows a schematic of this EMVD, and Fig. 3 shows a desirable transfer characteristic between the z and θ domains.

The benefit of using the resonant valve-spring system in the proposed EMVD is the same as that for using it in the NFEMVD: that the springs, ideally, allow lossless transitions of the valve from one end of the stroke to the other. For the valve-spring system, the forces are largest at the ends of the stroke because the spring forces increase linearly with valve displacement from the middle of the stroke. If the relationship between valve motion and motor shaft motion were linear (as in the MAEMVD), these large holding forces would make it difficult to hold the valve in the open or closed position without using large motor torques, and thus a lot of electrical power [7]. In addition, precise control of valve seating velocity would require precise control of motor

velocity. A cam profile such as that in Fig. 3 allows both these problems to be solved, as we see in the next section.

IV. System Modeling

A. Nonlinear Mechanical Transformer Relations

Because θ is a function of z and vice versa, it is easy to show that the use of the nonlinear mechanical transformer implies that the following relations hold between θ and z [7]:

$$z = f(\theta) \Longrightarrow \theta = f^{-1}(z) \tag{1}$$

$$\frac{dz}{dt} = \frac{dz}{d\theta}\frac{d\theta}{dt} \tag{2}$$

$$\frac{d^2z}{dt^2} = \frac{d^2z}{d\theta^2}\left(\frac{d\theta}{dt}\right)^2 + \frac{dz}{d\theta}\frac{d^2\theta}{dt^2}. \tag{3}$$

The nonlinear mechanical transformer provides a desirable coupling between the z and θ domains. By equating the power in the z and θ domains and using the NTF characteristic, the following relation results:

$$\tau_\theta = \frac{dz}{d\theta}F_z \tag{4}$$

where τ_θ is torque in the θ domain and F_z is the force in the z domain.

There are essential benefits obtained by using this nonlinear mechanical transformer. At either end of the stroke, the slope of the cam characteristic in (4), $(dz/d\theta)$, is very small. Thus, the reflected motor inertia in the z domain is very large, creating inherently smooth valve kinematics profiles because the valve is slowed down by the large effective inertia near the ends of the stroke. This characteristic makes it easier to control the motor velocity near the ends of the stroke. Moreover, the large spring forces at the ends of the stroke in the z domain are transformed into small torques in the θ domain by (4). In addition, because the gas force on the exhaust valve is largest at the opening end of the exhaust stroke, the reflected gas force in the θ domain obtained according to (4) is also small, making it easier to open the exhaust valve against a large gas force [7].

B. Equations of Motion for the EMVD

The equations of motion for the EMVD in Fig. 2 are as follows [7]:

$$F_z = m_z\frac{d^2z}{dt^2} + B_z\frac{dz}{dt} + K_z z \tag{5}$$

$$J_\theta\frac{d^2\theta}{dt^2} + B_\theta\frac{d\theta}{dt} + \tau_\theta = K_T i \tag{6}$$

where τ_θ is the transformer torque in the θ domain, F_z is the transformer force in the z domain, J_θ is the inertia in the θ domain, m_z is the mass in the z domain, B_θ is the friction in the θ domain, B_z is the friction in the z domain, K_T is the motor torque constant, K_z is the effective spring constant for the two springs, i is the motor current, θ is the displacement in the rotational domain, and z is the displacement in the vertical domain.

Equations (5) and (6) can be combined using the NTF characteristic relations (1)–(4). In this manner, we can obtain a single equation of motion in either the z or the θ domains. In the θ domain, if we are to assume a time-varying gas force disturbance also acts on the valve (typical of exhaust valves in an internal combustion engine), the resulting equation of motion is

$$\left(J_\theta + m_z\left(\frac{dz}{d\theta}\right)^2\right)\frac{d^2\theta}{dt^2} + \left(B_\theta + B_z\left(\frac{dz}{d\theta}\right)^2\right)\frac{d\theta}{dt} + \left(m_z\frac{dz}{d\theta}\frac{d^2z}{d\theta^2}\frac{d\theta}{dt}\right)\frac{d\theta}{dt} + K_z f(\theta)\frac{dz}{d\theta} = K_T i + g(\theta, t) \tag{7}$$

where $g(\theta, t)$ is the time-varying gas force acting on the valve reflected to the θ domain.

In effect, the system in (7) resembles a typical second-order time-varying differential equation with nonlinear mass/inertia and nonlinear damping. Assuming no inputs to the system (so $g(\theta, t) = 0$ and $i = 0$), the system has an equilibrium at $(z, \theta) = (0, 0)$, and assuming a flat slope for the *extended* ($|\theta| \geq 26^\circ$) cam characteristic in Fig. 3 at the ends of the stroke, it has an infinite number of equilibria at the ends of the stroke for ($z = 4$ mm,$|\theta| \geq 26^\circ$). The presence of these equilibria can be shown with standard energy-derived Lyapunov functions [26].

For the model in (7), it is important to note that because $(dz/d\theta)$ is different for each point in the valve stroke, the dynamic characteristics of the EMVD change at every point in the stroke. In the θ domain, the effective system gain of the valve-spring system increases at the ends of the stroke and decreases at the midpoint of the stroke.

From the EMVD model in (7), if we assume there is no gas force acting on the engine valve, we can derive linearized system equations for the EMVD. For example, at the ends of the stroke where the motor is essentially decoupled from the engine valve-spring system (because the cam slope is almost 0), the EMVD equation of motion reduces to

$$J_\theta\ddot{\theta} + B_\theta\dot{\theta} = K_T i. \tag{8}$$

In the middle of the stroke, assuming the slope of the NTF relation is equal to the constant r, the EMVD equation of motion reduces to

$$(J_\theta + m_z r^2)\ddot{\theta} + (B_\theta + B_z r^2)\dot{\theta} + K_z r^2\theta = K_T i. \tag{9}$$

By taking the Laplace transform of (8) and (9), we obtain linearized transfer (functions from the input (current i) to the output (motor position θ) for the EMVD plant at the ends of the stroke and at the middle of the stroke, respectively

$$G_{\text{end-of-stroke}}(s) = \frac{K_T}{J_\theta s^2 + B_\theta s} \tag{10}$$

$$G_{\text{midstroke}}(s) = \frac{K_T}{(J_\theta + m_z r^2)s^2 + (B_\theta + B_z r^2)s + K_z r^2}. \tag{11}$$

The linearized transfer function in (10) is only valid for small displacements near the ends of the stroke, whereas that of (11) is only valid for small displacements about the middle of the stroke.

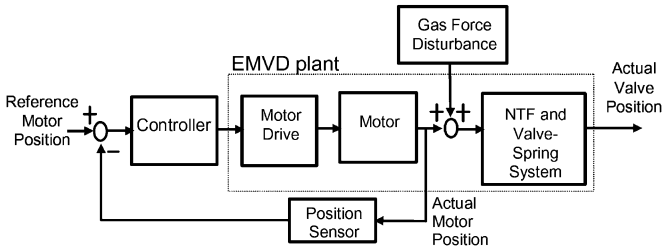

Fig. 4. Block diagram of the feedback-controlled EMVD apparatus. The EMVD plant is comprised of the motor drive, motor, nonlinear mechanical transformer, and the valve-spring system.

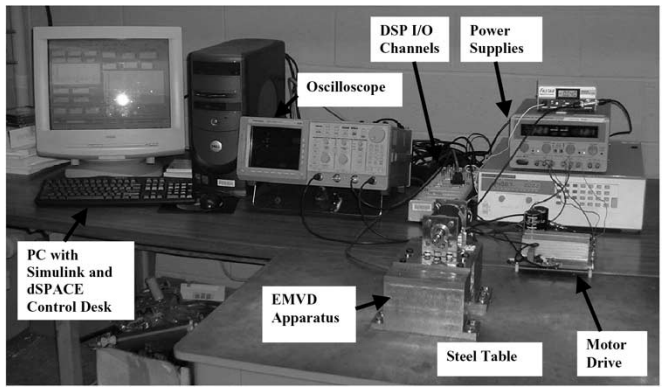

Fig. 5. EMVD experimental test stand, showing the EMVD apparatus and supporting equipment.

V. Design and Control Considerations

A block diagram of the feedback-controlled EMVD apparatus is shown in Fig. 4. The reference input is the desired motor position, and the system output is actual motor position. The difference between the actual motor position and the reference position is passed into a controller that provides a current control input to the motor drive. The motor drive then supplies the desired current to the motor. because the nominal values of the system parameters in (7) are either known or can be determined experimentally, it is possible to design and implement various types of controllers for the EMVD. On initial consideration, there are a number of important issues in the controller design.

1) We have established that the plant is fundamentally nonlinear. Optimal performance will almost certainly require nonlinear control.
2) Because of the importance of soft landing, it seems essential that the control be precise near the end of the valve closing stroke.
3) The controller will control valve position, with opening and closing transitions occurring when the controller is given a reference position that describes an idealized free-flight trajectory. In this respect, the controller detects the effects of friction and gas loads as position error. The controller should be able to keep position error small in the presence of these variable loads and also in the presence of parameter variation.
4) To function in a modern gasoline engine, a transition time of 3.5 ms or less must be achieved [6]. Thus, the required natural frequency of the valve-spring system in the EMVD is approximately 100 Hz.

In practice, we find that considerations (1) and (2) are not so important. Although a nonlinear controller has been proposed [26]–[28], we report quite good results obtained with fixed-gain linear controllers.

By using an extremely flat slope for the extended cam profile at the ends of the valve stroke (1), and by implementing position control in the θ domain, low closing velocity can be achieved without especially precise position control. The reason for this characteristic is that by using a flat slope for the extended cam profile, the motor can continue to rotate past $|\theta| \geq 26^\circ$ in the θ domain, whereas the valve stays at a fixed position ($|z| = 4$ mm) in the z domain. In addition, this flat slope also allows for the valuable zero holding current characteristic in the EMVD. Note that this combination of design features results in almost no ability to alter the z domain position at the end of the stroke. If the valve were to come to rest just short of the closed position, as would happen if either the controller fails or there is no lash-adjustment device in the EMVD, there may be no low-power control action that will correct the situation. The solution to this problem is very accurate adjustment of the valve actuator position, probably incorporating some sort of automatic motor position self-adjustment included in the control algorithm.

On our first attempt at controller design, we achieved the desired 3.5-ms transition time using fixed-gain linear controllers, but we were able to do so largely by selecting suitably stiff springs and suitably low system inertias. We have yet to demonstrate that the controller will perform well when compensating for a large gas load.

VI. The Experimental EMVD Test Stand

To prove the concept of the proposed EMVD, an experimental apparatus was designed, constructed, and integrated into a computer-controlled experimental test stand. In this section, we describe the components in the EMVD apparatus and discuss its structure. For more details on the EMVD test stand, see [30].

The test stand is comprised of a computer-controlled DSP (the DS1104 from dSPACE, Novi, MI,) to control the EMVD, a motor drive circuit to process the control signal from the DSP and drive the motor, the EMVD apparatus, appropriate linear and angular displacement sensors, and supporting measurement devices, including an oscilloscope to measure and display relevant experimental waveforms. Fig. 5 shows a picture of the constructed EMVD test stand.

There were three constraints on the design of this experimental test stand. First, the mass and inertia of the moving components in the apparatus, for example, of the valve, should be as small as possible. This is because the required spring constants and forces grow proportionally with the mass/inertia of components in the system. Second, to achieve an overall system bandwidth of about 1 kHz, the bandwidth of the motor drive and sensors should be at least 10 kHz, such that they did not greatly affect the overall feedback-controlled system dynamics. Third, the use of off-the-shelf components was dictated

wherever possible to minimize the time required for designing our own components and for constructing the test stand.

We decided not to include two important devices in the experimental test stand. First, a gas-force simulator was not included because the test stand was only intended as a proof of concept for the proposed EMVD. Second, a lash-adjustment device was also not included in the EMVD apparatus. In the near future, a gas-force simulator will be added to the experimental test stand. We have also completed the design of a lash-adjustment device [28] and will begin testing it soon. Once both these devices are incorporated into the experimental test stand, we will carry out experiments with gas-force, and quantify the performance of the EMVD and the lash-adjustment device under gas-force disturbances. Design considerations and results from these experiments will be presented in a future publication.

One of the most critical components in the experimental test stand was the motor. We obtained an off-the-shelf permanent magnet low-inertia dc motor (the 4N63–100 from Pacific Scientific, Rockford, IL, USA) with adequate characteristics—a large torque-to-rotor inertia ratio $(2.543 \cdot 10^5 (1/s^2))$, high rated power output (321 W), appropriate rated speed (3440 rpm), appropriate rated rms (14.2 A) and pulse (48 A) current, appropriate rated voltage (42 V), and appropriate electrical (0.11 ms) and mechanical (0.6 ms) time constants—for the proposed EMVD. Unfortunately, this motor is large in size—too large to be easily implemented in an actuation system on an IC engine head. Smaller motors will be required to implement the proposed EMVD on an engine cylinder head [30]. To this end, a very small off-the-shelf dc motor (the B1118-050-A from Portescap, West Chester, PA, USA) capable of actuating engine intake valves and small enough to be implemented on an IC engine head was more recently obtained. Design considerations and experimental results obtained using this motor will be presented in a future publication.

To achieve the intended control system bandwidth, a high-bandwidth motor drive circuit realizing hysteretic current control [31], [32] has been developed; details of this design can be found in [29].

To meet the 100-Hz natural frequency requirement of the valve-spring system, die springs having the appropriate stiffness were selected. We obtained a soft (stiffness $= 5.031$ kN/m) spring set and a stiff (stiffness $= 56.096$ kN/m) spring set. We picked the stiff springs to allow for 3.5-ms transition times, and we designed the EMVD apparatus for this set of springs. The soft spring set was picked so we could use it to carry out preliminary controller design and to verify the operation of the EMVD with longer transition times and lower force levels. In the EMVD apparatus, these spring sets were used together with standard exhaust engine valves from a 16- valve, 2.0-L Zetec cylinder head (Ford Motor Company, Detroit, MI, USA).

An E6D differential optical encoder with a 8192-line resolution (US Digital, Vancouver, WA) was selected for rotary position sensing, whereas a high-bandwidth, low-mass, variable reluctance-type linear position sensor (Fastar FS300 from Sentech, Fort Washington, PA, USA) was obtained for measuring valve displacement in the z domain.

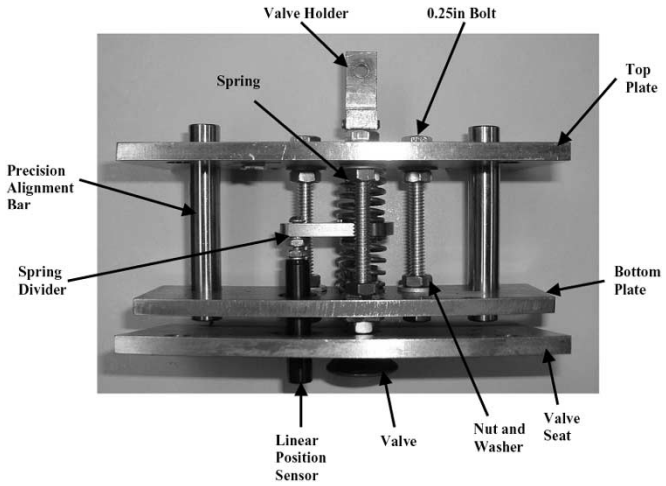

Fig. 6. Valve assembly with the soft spring set.

The disk cam is the most important part in this EMVD apparatus. The disk cam is the nonlinear mechanical transformer element that provides the unique features of this valve drive. The cam was press-fit onto the motor shaft. We obtained a CFS-5-V roller follower (IKO International, Parsippany, NJ, USA) to connect the valve holder (at the top of the valve stem) to the disk cam. For the smooth profile of the center of the roller follower in the disk cam slot, we decided to implement the continuous function

$$z = f(\theta) = (0.004 \text{ m}) \frac{\sin(0.06039\theta)}{\sin(0.999\pi/2)} \tag{12}$$

for $-26^\circ \leq \theta \leq 26^\circ$. In (12), θ is in radians and the sine functions take their arguments in radians.

In the EMVD apparatus, the valve-spring system is carried in a larger subassembly called the valve assembly. In addition to the valve and springs, the valve assembly contains the plates, which constrain the stationary ends of the springs (the top and bottom plates), valve guides, a plate with a valve seat, guide pins, and a linear position sensor. We assembled two valve assemblies, the first with stiff springs and the second with soft springs. Fig. 6 shows the assembled valve assembly. The spring divider is rigidly connected to the valve stem, and the top and bottom plates are rigidly held together by 0.25-in. bolts.

The assembled experimental apparatus is shown in Figs. 7 and 8. The entire apparatus is mounted on a table, with two supporting columns. The motor is mounted onto one of these columns with two motor mounting brackets. The optical encoder is mounted on the rear end of the motor shaft. The top plate and valve seat of the valve assembly are rigidly mounted to the two columns.

Fig. 7 shows the apparatus without column II obstructing the view. From this figure, we can easily imagine the proposed EMVD in operation. As the motor shaft is rotated either clockwise or counterclockwise, the disk cam—which is rigidly connected to the motor shaft—also rotates, causing the roller-follower to move within the disk cam slot. When the roller-follower moves, the engine valve, which is connected to

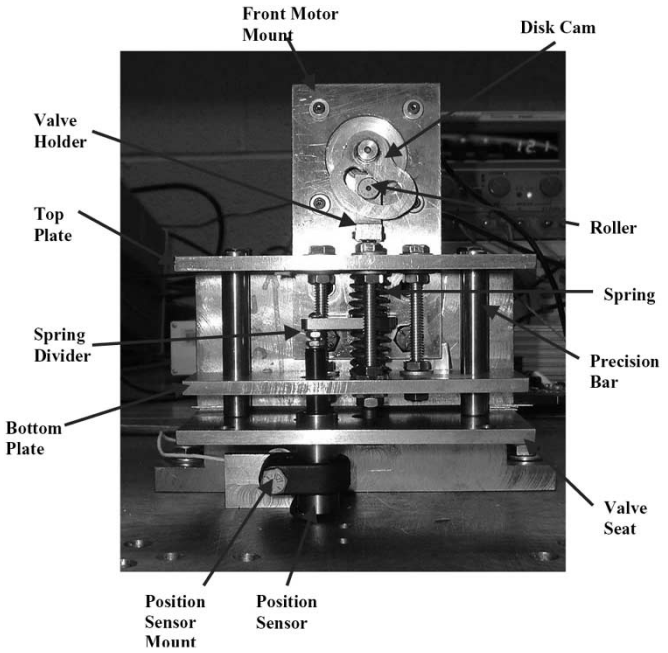

Fig. 7. Front view of the EMVD apparatus, showing the disk cam and the valve-spring system. The precision bars were used to align the valve-spring system.

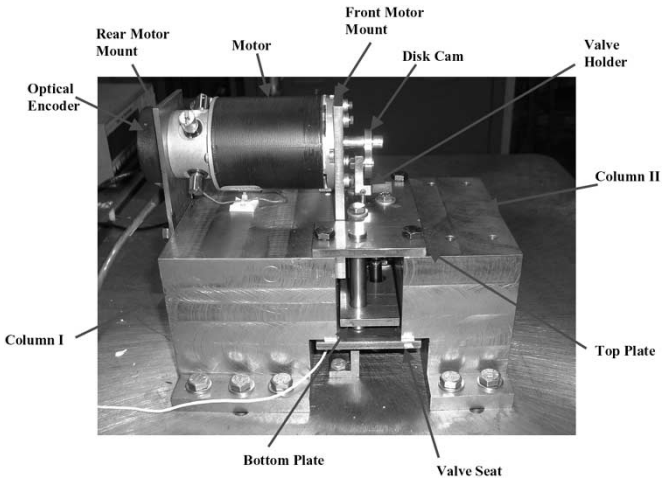

Fig. 8. Side view of the constructed EMVD apparatus.

the roller-follower by the valve holder, moves vertically up or down.

At either end of the disk cam slot (the end of the valve stroke), the slope of the cam characteristic in (4), $(dz/d\theta)$, is very small, and thus, the engine valve can be held open and closed with a near-zero motor current.

VII. Controller Design and Experimental Results

A. Overview

As shown in Fig. 9, there are three modes of engine valve motion in the EMVD that must be controlled: the initial, holding, and transition modes. The initial mode controller moves the engine valve from its resting position at the middle of the stroke

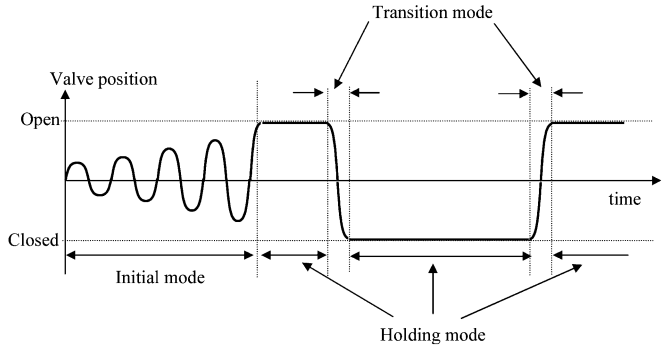

Fig. 9. Three modes for the EMVD: initial, holding, and transition modes.

TABLE I
Summary of Parameters for the Pacific Scientific 4N63-100 Motor

Parameter	Manufacturer's Specifications	Experimental Value
Resistance, R_m (Ω)	$0.89@25^oC$	0.993
Torque constant, K_T ($\frac{\text{Nm}}{\text{A}}$)	0.07	0.0694
Back EMF constant, K_ω ($\frac{\text{V}}{\text{rad/s}}$)	0.07	0.0696
Viscous friction, B_m ($\frac{\text{Nm}}{\text{rad/s}}$)	$7.64 \cdot 10^{-5}$	$1.85 \cdot 10^{-4}$
Inductance, L_m (μH)	100	120
Inertia, J_m (kgm^2)	$3.6 \cdot 10^{-6}$	$5.185 \cdot 10^{-6}$

TABLE II
Motor Drive Circuit Parameters

Quantity	Desired Value	Measured Value
Slew rate	$\approx$70 A/ms	$\approx$400 A/ms
Bandwidth	10 kHz	9.5 kHz
Power	1 kW	$\geq$1 kW
Current ripple	$\leq$1 A	0.98 A

to one end of the stroke. The holding mode controller is used to hold the valve at either end of the stroke with a variable holding time. The transition mode controller is used to move the valve from one end of the stroke to the other. The transition mode controller also minimizes error during valve transitions, such that the valve is closed with a small seating velocity.

We implemented different controllers for the soft and stiff spring-based EMVD apparatuses. For the soft spring set, we used a refined reference input and a single transition mode controller to carry out initial, holding, and transition mode control. For the stiff spring-based EMVD apparatus, we implemented an initial mode controller and a separate transition mode controller to carry out both holding and transition mode control, relying on a refined reference position input to allow this controller to carry out both holding and transition control functions.

B. System Identification Experiments

Before designing any controllers, we first performed system identification experiments to extract parameters for the EMVD plant and characterize both the soft and stiff spring-based EMVD apparatuses.

We tested the motor and motor drive before experimenting with the EMVD apparatus itself because we needed to confirm that the motor and motor drive were suitable for the application. Table I shows a summary of the motor parameters obtained experimentally. From the table, we can see that, in general, the measured characteristics of the motor are close to the

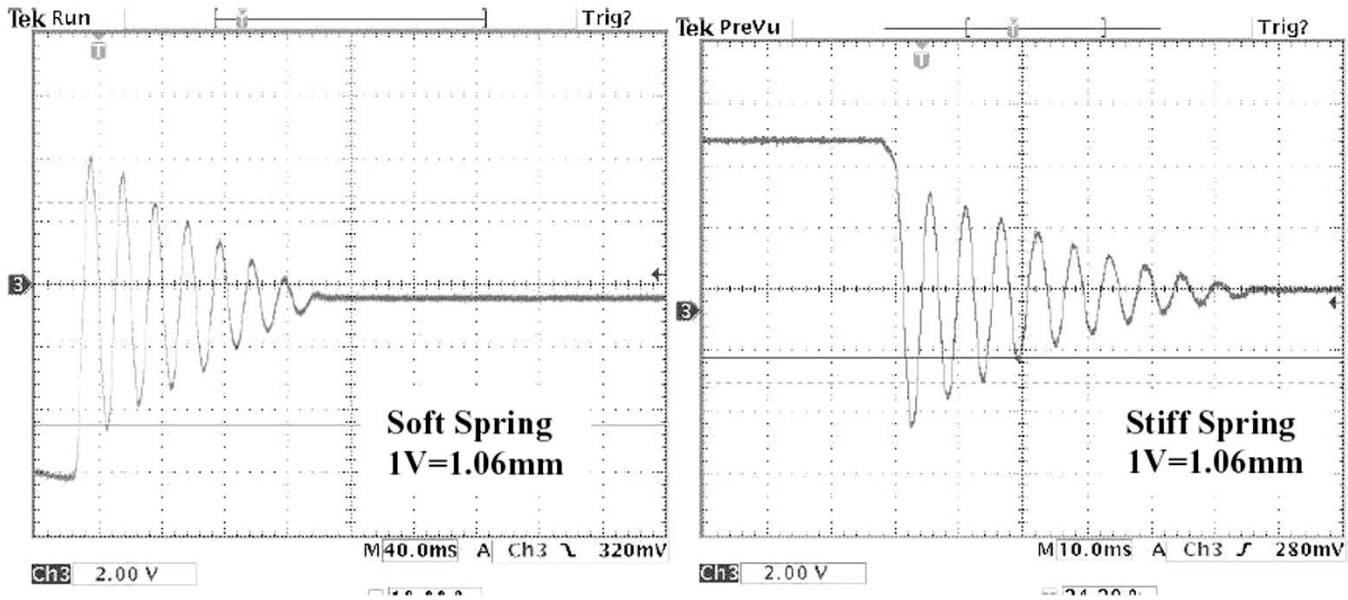

Fig. 10. Free oscillation of valve assembly with the soft and stiff spring sets.

manufacturer's specifications. However, the motor viscous friction coefficient is a little more than two times larger than the manufacturer's specifications. It is possible that the motor shaft was somehow misaligned during testing, increasing the drag between the shaft and the motor bearings. It is also possible that the additional friction was due to drag on parts connected to the motor; however, we were not able to experimentally determine this friction. The measured rotor inertia for the motor was 1.4 times that specified by the manufacturer. The error in measured inertia is probably directly related to the error in measured friction because inertia is deduced from the motor's mechanical time constant.

The motor drive design parameters measured in the laboratory together with the design targets are shown in Table II. Based on the rapid response and high slew rate of the motor drive, we concluded that at least in terms of controller design, the hysteresis current-controlled motor drive can be treated as a linear gain between the reference motor current and the actual motor current. This approximation is justified because the ripple current in the motor drive output is always above 200 kHz and can thus be treated as a low-amplitude, high-frequency disturbance that is filtered by the motor. For more details on the motor and motor drive experimental tests, see [29] and [30].

The free oscillation experiments were carried out to determine the quality factor (2π multiplied by the ratio of the maximum energy stored in the system to the total energy lost in each closed-to-opened-to-closed transition [33], Q, the approximate damped natural frequency, ω_{d}, and the damping ratio for the engine valve-spring system. It is important to note that the higher the Q for the EMVD plant, the lower the losses and the less the strain on the motor driving the engine valve-spring system. In addition, we planned to use the experimental value of ω_{d} to generate a reference input for the feedback-controlled EMVD.

For the stiff spring-based apparatus, the experimental motor parameters in Table I were used with the free oscillation

TABLE III
FREE OSCILLATION EXPERIMENT PARAMETERS FOR THE EMVD PLANT

	Soft Spring	Stiff Spring
Q	13.33	15.63
ω_{d}	51 Hz	185 Hz
ζ	0.0332	0.0375

experimental results described here to obtain coefficients for linearized transfer functions with forms matching (10) and (11). For the soft spring-based apparatus, we carried out open-loop experiments to obtain linearized transfer functions matching those in (10) and (11). Based on the linearized transfer functions obtained via system identification experiments, different linear controllers were designed to control the soft spring and stiff spring-based EMVD apparatuses.

The experiments characterized the free oscillation dynamics of the valve assembly after releasing the valve from one end of the stroke. Fig. 10 and Table III show the data from this experiment with associated values of quality factor, damped natural frequency, and damping ratio. As expected, Q and ω_{d} were higher with the stiffer spring set than with the soft spring set, and the losses were not too high (approximately 27% per cycle with the stiffer spring set) for both valve assemblies.

Using the parameters in Tables I and III, as well as laboratory measurements of the z domain mass, the following linearized transfer functions, from current i to motor position θ, were obtained for the stiff spring-based EMVD apparatus:

$$G_{\text{end-of-stroke,stiff}}(s) = \frac{0.069}{4.87 \cdot 10^{-6} s^2 + 0.0099 s} \tag{13}$$

$$G_{\text{midstroke,stiff}}(s) = \frac{0.069}{1.2 \cdot 10^{-5} s^2 + 1.3 \cdot 10^{-3} s + 5.4}. \tag{14}$$

TABLE IV
SOFT SPRING BASED EMVD PARAMETERS FROM CURVE FITTING TO EXPERIMENTAL DATA

Parameter	Experimental Value	Expected/Calculated Value
J_{motor}	$4.15 \cdot 10^{-6}\text{kgm}^2$	$3.5 \cdot 10^{-6}\text{kgm}^2$
$J_{\text{disk cam}}$	Assumed to be $\approx 0.728 \cdot 10^{-6}\text{kgm}^2$	$0.72 \cdot 10^{-6}\text{kgm}^2$
J_θ	$4.87 \cdot 10^{-6}\text{kgm}^2$	$4.22 \cdot 10^{-6}\text{kgm}^2$
K_{T}	$0.069 \frac{\text{Nm}}{\text{A}}$	$0.07 \frac{\text{Nm}}{\text{A}}$
B_θ	$9.9 \cdot 10^{-3} \frac{\text{Nm}}{\text{rad/s}}$	$7.64 \cdot 10^{-5} \frac{\text{Nm}}{\text{rad/s}}$
m_z	95.9 g	≈ 90 g
B_z	$37.8 \frac{\text{kg}}{\text{s}}$	$20 \frac{\text{kg}}{\text{s}}$
K_z	$1.182 \cdot 10^4 \frac{\text{N}}{\text{m}}$	$1.653 \cdot 10^4 \frac{\text{N}}{\text{m}}$

We carried out two open-loop transfer function experiments for the soft spring-based EMVD apparatus. The experimental setup for the first experiment was as follows: a sinusoidal current command was input to the motor drive. The frequency of this sinusoidal current command was increased in increments of a few Heartz, and the amplitude of this commanded current was adjusted such that motor displacement amplitude was less than 0.1 rad about the middle of the stroke. The amplitudes of the motor current and motor position were recorded. The phase difference between these two signals was also recorded. The experimental data was curve fit to a transfer function of the form given in (10). In this transfer function, the value of K_{T} was assumed to be 0.069 Nm/A, as determined in the motor testing experiments.

Table IV shows the experimental results in which the parameters were obtained by comparison to the model in (10). Equation (15) shows the curve fitted transfer function (from i to θ) that was found

$$G_{\text{end-of-stroke,soft}}(s) = \frac{0.069}{4.87 \cdot 10^{-6}s^2 + 0.0099s}. \tag{15}$$

As mentioned earlier, at the ends of the stroke, the engine-valve spring system can be assumed to be decoupled from the motor, and thus the parameters in Table IV are essentially motor parameters. This is also why transfer functions (13) and (15) are identical, even though they apply to systems with different springs.

The experimental setup for the second open-loop transfer function experiment was essentially the same as the first experiment described previously, except that the roller-follower was placed in the disk cam slot and connected to the valve assembly. As before, the experimental data was curve fit to a transfer function of the form given in (11).

The experimental results obtained for the second experiment are also displayed in Table IV, but in this case the parameters were obtained by comparison to the model in (11). Equation (16) shows the curve fitted transfer function from i to θ

$$G_{\text{midstroke,soft}}(s) = \frac{0.069}{2.26 \cdot 10^{-5}s^2 + 0.0029s + 1.0935}. \tag{16}$$

The actual mass in the z domain closely matched the expected mass, whereas the friction in the z domain was about 1.6 times larger than expected. Furthermore, the spring constant in the z domain, K_z, was much smaller than that expected. One possible reason for these results is that the disk cam had been worn out when this experiment was performed, causing the deterioration of the desired nonlinear cam profile. It is also possible that there were some misalignments in the apparatus.

C. Initial Mode Control

When the EMVD is at rest, the engine valve is at the $\theta = 0$ position. The objective of the initial mode controller is to move the valve from this resting position to one end of the stroke ($\theta \approx 0.46$ rad) in as short a time period as possible.

For the soft spring-based EMVD, the transition mode controller was used to carry out initial, holding, and transition mode control. To carry out initial mode control for this system, a sinusoidal motor position reference input with linearly increasing amplitude was created. Using this reference input, any well-designed transition mode controller applies pulses of current to the motor, causing the disk cam to oscillate sinusoidally at a linearly increasing amplitude, thereby enabling initial mode control.

For the stiff spring-based EMVD apparatus, the need for a fast initial mode transient is particularly important because the initialization time must be much smaller than the thermal time constant of the motor. Optimally, for the fastest EMVD startup transients, pulses of current must be applied to the motor at the exact moment when the motor velocity changes sign, such that the number of cycles required to increase the motor position amplitude to full-stroke amplitude is minimized. Such an initial mode control law is given by

$$i_{\text{m}} = \alpha \frac{\omega_{\text{m}}}{|\omega_{\text{m}}|} \tag{17}$$

where α is a constant.

Fig. 11 shows the initial mode control transient for the stiff-spring based EMVD apparatus, using (17) with $\alpha = 7$ A. After the initial mode control period (35 ms), the controller is switched from the initial mode controller to the transition/holding mode controller.

D. Holding Mode Control

The objective of the holding mode controller is to hold the engine valve at either the open or the closed position for a variable time period. However, holding mode only requires a carefully generated motor position reference input and a suitable transition mode controller. Thus, by using a reference input that is latched/held at one extreme amplitude during the holding period, any well-designed transition mode controller can carry out holding mode control.

E. Transition Mode Controllers

The main constraint on the design of the transition mode controllers was that they have fairly high bandwidth (at least 300 Hz for the system with soft springs and 1 kHz for the system with stiff springs). Because the EMVD plant's linearized transfer function at the ends of the valve stroke resembles that of a dc motor, which has an integrator to eliminate steady state errors in position, we did not need to use an integrator in our controller. Thus, lead compensators were designed and implemented for

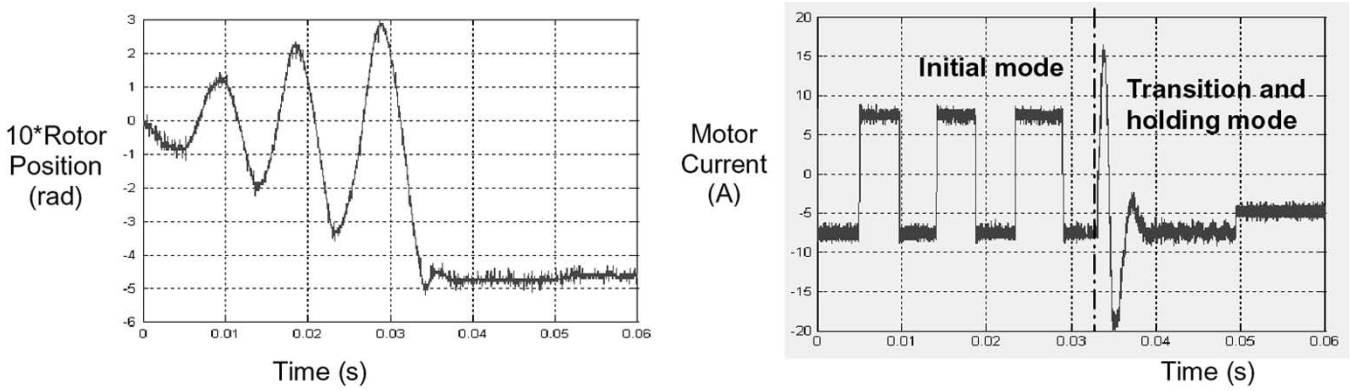

Fig. 11. Experimental waveforms during initial mode control. The initial mode transient was completed in 35 ms with ± 8 A current pulses, and required an average electrical power of 150 W.

the EMVD apparatus; the design and implementation of these controllers is described next.

F. Lead Compensator Design

For a typical lead compensator, the transfer function, $G_{\text{LEAD}}(s)$, is given by

$$G_{\text{LEAD}}(s) = K\frac{1+\frac{1}{z_{\text{LEAD}}}s}{1+\frac{1}{p_{\text{LEAD}}}s} \tag{18}$$

where K is the controller gain, z_{LEAD} is the lead compensator zero location, and p_{LEAD} is the lead compensator pole location. These three constants are chosen to obtain the desired transient response for the feedback-controlled EMVD plant. For the initial design of the lead compensator for the soft spring-based EMVD, we set $K = 400$, $z_{\text{LEAD}} \approx 1709$ rad/s, and $p_{\text{LEAD}} \approx 7754$ rad/s, to obtain the desired feedback-controlled response at both mid-stroke and end-stroke. Simulations of the system transient response were used to confirm the operation of the controller. The control bandwidth was estimated to be 450 Hz from Bode plots of the feedback-controlled system.

The lead compensator was implemented and run on the DSP with a sampling rate of 15 kHz and a fourth-order fixed step Runga-Kutta differential equation solver. We varied the chosen zero/pole locations and the controller gain until we were satisfied with the feedback-controlled EMVD response. The lead compensator that gave the best feedback-controlled performance is given by the following transfer function:

$$G_{\text{LEAD}}(s) = 350\frac{1+5.85\cdot 10^{-4}s}{1+1.22\cdot 10^{-4}s} \tag{19}$$

which corresponds to a controller gain of 350, a zero location of 1709.4 rad/s, and a pole location of 8196.7 rad/s.

Using the same empirical technique, we designed a lead compensator for the stiff spring-based EMVD plant. The lead compensator that gave the best feedback-controlled performance is given by the following transfer function [28]:

$$G_{\text{LEAD}}(s) = 250\frac{1+8\cdot 10^{-4}s}{1+2\cdot 10^{-4}s} \tag{20}$$

which corresponds to a controller gain of 250, a zero location of 1250 rad/s, and a pole location of 5000 rad/s. From Bode plots of the feedback-controlled system, the control bandwidth was estimated to be 850 Hz.

G. Feedback-Controlled Experimental Results

The lead compensators (19) and (20) were implemented in the EMVD test stand. In the laboratory, we observed that although the dynamics of the EMVD plant do change between the middle and end of the stroke, this change is not great enough to affect these fixed-gain linear controllers' performances.

For the soft spring-based EMVD, in addition to the lead compensator, 2.25 A pulses of (feed-forward) current were injected at the start of the valve transitions from the open-to closed or closed-to-open positions, respectively, to see if we could reduce valve transition time significantly by moving the roller off the ends of the cam with a larger initial velocity. The current pulses did not change valve transition time significantly, and the experimental results obtained without using these pulses are identical to those presented here. Furthermore, the valve was held for 0.25 s at each end of the stroke. The lead compensator (19) was used together with a carefully generated reference input (a 35-Hz sine wave that was latched at its positive and negative maxima for a fixed time period to hold the valve closed and opened, respectively) to obtain initial, holding, and transition mode controls.

Fig. 12 shows the motor position and current for the lead compensated soft spring-based EMVD. For this experiment, a 12.8 ms transition time was observed. The peak motor current was approximately 4 A, and the motor current waveform obtained is close to that expected for a hysteresis current-controlled motor drive. Although not shown in the figure, the average power during the valve transition period was approximately 12 W, whereas that during the holding period was approximately 5 W. The holding current for the EMVD was not the predicted 0 A because of misalignments in the EMVD apparatus.

Fig. 13 shows the motor position, valve position, and motor current for the lead compensated stiff spring-based EMVD. For this experiment, a 96-Hz sine wave (latched at its positive and negative maxima for a fixed time period to hold the valve

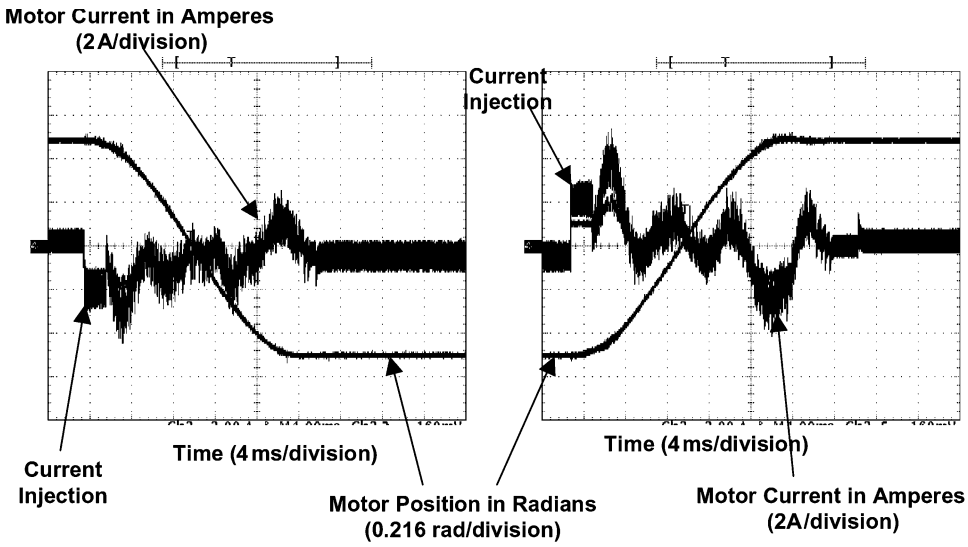

Fig. 12. Experimental results for the transition mode with 12.8 ms transition time.

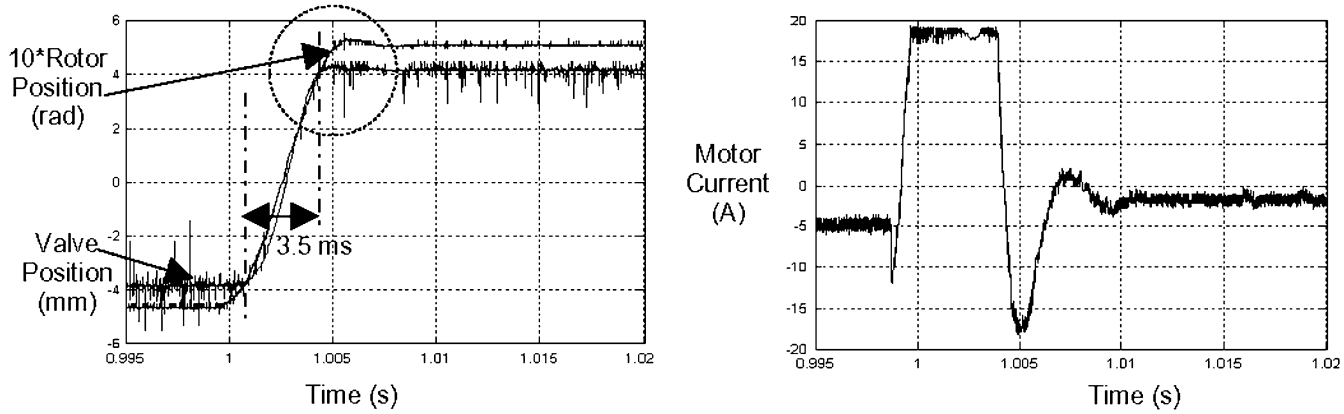

Fig. 13. Experimental results for the transition mode showing the 3.5-ms transition time. Zero holding current was observed after power to the motor was shut off.

closed and opened, respectively) was used as the reference input, and 3.5-ms transition times were observed, corresponding to performance levels sufficient for 6000-rpm engine speeds. Although there is overshoot in the θ domain because the nonlinear cam profile (12) is used, there is no overshoot in the z domain. The saturation in the first part of the current profile in Fig. 13 is due to the 20 A current limit on the motor drive. Based on the current profile seen here, the total estimated electrical power consumption of the stiff spring-based EMVD in a typical 2.0-L, 16-valve engine operating at 6000 rpm under full-load (wide-open-throttle) conditions is 2.56 kW, which is on the same order as that of the mechanical power consumption of a conventional camshaft-driven valve train assuming 50% alternator efficiency [28]. This estimation was carried out by adding the actual actuator power consumption we obtained experimentally to an estimation of the additional work the actuator would need to do to overcome the gas forces present when actuating exhaust valves at 6000-rpm engine speeds in the wide-open throttle condition. The nonzero holding current (which results from a small non-zero position error being supplied to the controller) in Fig. 13 is below that required to overcome static friction in the motor, thus, when the motor drive was turned off during the holding mode, the valve was still held at one end of the stroke.

Using the linear position sensor, we estimated valve seating velocities for the soft spring-based EMVD apparatus as ranging between 3 and 17 cm/s. Because our linear position sensor did not work for faster valve transition times, we used a high-speed camera to measure the seating velocity of the stiff spring-based EMVD apparatus; the seating velocity was repeatedly measured and ranged between 15.5 and 27.2 cm/s. These seating velocities are encouraging because they show that the EMVD does indeed meet the seating velocity constraints mentioned earlier.

The seating velocities obtained are comparable to those that have been obtained for the NFEMVD [21], [23]–[25], and the estimated power consumption is much lower than that for the MAEMVD [15], [16]. The estimated power consumption for the NFEMVD under full-load conditions is not known [21].

VIII. Conclusion

The objectives of this research were to construct an EMVD apparatus in the laboratory, integrate it into a

computer-controlled experimental test stand, and carry out experiments to verify the operation of this apparatus. All three objectives were fulfilled. The experimental results obtained using the test stand are very promising. Fast transition times, low seating velocities, zero holding power, and low average power consumption have been demonstrated. In addition, the experimental results offer key insights on how to improve the apparatus in the future. In particular, in the near future, a smaller dc motor, a gas force simulator, and a lash-adjustment device will be incorporated into the EMVD experimental test stand.

REFERENCES

[1] F. Pischinger and P. Kreuter, "Electromagenetically operated actuators," U.S. Patent 4 455 543, 1984.

[2] M. Pischinger, W. Salber, F. van der Staay, H. Baumgarten, and H. Kemper, "Benefits of electromechanical valve train in vehicle operation," *SAE Tech. Paper Series*, 1996.

[3] J. G. Kassakian, H.-C. Wolf, J. M. Miller, and C. J. Hurton, "Automotive electrical systems circa 2005," *IEEE Spectrum*, pp. 22–27, Aug. 1996.

[4] M. B. Levin and M. M. Schlecter, "Camless engine," *SAE Tech. Paper Series*, 1996.

[5] P. Barkan and T. Dresner, "A review of variable valve timing benefits and modes of operation," *SAE Tech. Paper Series*, 1989.

[6] T. Ahmad and M. A. Theobald, "A survey of variable-valve-actuation technology," *SAE Tech. Paper Series*, 1989.

[7] W. S. Chang, T. A. Parlikar, J. G. Kassakian, and T. A. Keim, "An electromechanical valve drive incorporating a nonlinear mechanical transformer," *SAE Tech. Paper Series*, 2003.

[8] R. Steinberg, I. Lenz, G. Koehnlein, M. Scheidt, T. Saupe, and W. Buchinger, "A fully continuous variable cam timing concept for intake and exhaust phasing," *SAE Tech. Paper Series*, 1998.

[9] L. Mikulic, J. Schommers, B. Geringer, K. Wolf, and C. Enderle, "Variable gas exchange systems for S.I. engines—Layout and experimental data," *SAE Tech. Paper Series*, 1992.

[10] H. Nakamura, T. Nakashima, H. Aihara, and M. Ookubo, "Development of gear parts for VVT unit," *SAE Tech. Paper Series*, 1997.

[11] L. A. Gould, W. E. Richeson, and F. L. Erickson, "Performance evaluation of a camless engine using valve actuators with programmable timing," *SAE Tech. Paper Series*, 1991.

[12] F. Pischinger and P. Kreuter, "Arrangement for electromagnetically operated actuators," U.S. Patent 4 515 343, May 7, 1985.

[13] L. Brooke, "Camless BMW engine still faces hurdles," *Auto. Ind.*, p. 34, Oct. 1999.

[14] R. Flierl and M. Klüting, "The third generation of valvetrains—New fully variable valvetrains for throttle-free load control," *SAE Tech. Paper Series*, 2000.

[15] M. A. Theobald, B. Lesquesne, and R. R. Henry, "Control of engine load via electromagnetic valve actuators," *SAE Tech. Paper Series*, 1994.

[16] R. R. Henry and B. Lesquesne, "A novel, fully-flexible, electro-mechanical engine valve actuation system," *SAE Tech. Paper Series*, 1997.

[17] R. R. Henry and B. Lesquesne, "Single-cylinder tests of a motor-driven, variable-valve actuator," *SAE Tech. Paper Series*, 2001.

[18] S. Birch, "Renault research," *Automot. Eng. Int.*, p. 114, Mar. 2000.

[19] S. Butzmann, J. Melbert, and A. Koch, "Sensorless control of electromagnetic actuators for variable valve train," *SAE Tech. Paper Series*, 2000.

[20] M. Gottschalk, "Electromagnetic valve actuator drives variable valvetrain," *Des. News*, Nov. 1993.

[21] W. Hoffmann, K. Peterson, and A. Stefanopoulou, "Iterative learning control for soft landing of electromechanical valve actuator in camless engines," *IEEE Trans. Control Syst. Technol.*, vol. 11, no. 2, pp. 174–184, Mar. 2003.

[22] M. Montanari, F. Ronchi, C. Rossi, and A. Tonielli, "Control of a camless engine electromechanical actuator: Position reconstruction and dynamic performance analysis," *IEEE Trans. Ind. Appl.*, vol. 51, no. 2, pp. 1508–1519, Apr. 2004.

[23] Y. Wang, T. Megli, M. Haghgooie, K. S. Peterson, and A. G. Stefanopoulou, "Modeling and control of electromechanical valve actuator," *SAE Tech. Paper Series*, 2002.

[24] K. Peterson and A. Stefanopoulou, "Rendering the electromechanical valve actuator globally asymptotically stable," in *Proc. 42nd IEEE Conf. Decision and Control*, Maui, HI, Dec. 2003, pp. 1753–1758.

[25] 4 M. S. Ashhab, A. G. Stefanopoulou, J. A. Cook, and M. Levin, "Camless engine control for robust unthrottled operation," *SAE Tech. Paper Series*, 2000.

[26] J.-J. Slotine and W. Li, *Applied Nonlinear Control*. Upper Saddle River, NJ: Prentice-Hall, 1991.

[27] J.-J. Slotine and J. A. Coetsee, "Adaptive sliding controller synthesis for nonlinear systems," *Int. J. Control*, vol. 43, no. 6, 1986.

[28] W. S. Chang, "An electromechanical valve drive incorporating a nonlinear mechanical transformer," Ph.D. dissertation, Massachusetts Institute of Technology, Cambridge, Jul. 2003.

[29] T. A. Parlikar, "Experimental implementation of an electromagnetic valve drive,", S. M. thesis, Massachusetts Institute of Technology, Cambridge, Feb. 2003

[30] W. S. Chang, T. A. Parlikar, M. D. Seeman, D. J. Perreault, J. G. Kassakian, and T. A. Keim, "A new electromagnetic valve actuator," in *IEEE Workshop on Power Electronics in Transportation*, Auburn Hills, MI, Oct. 2002, pp. 109–118.

[31] D. M. Brod and D. W Novotny, "Current control of VSI-PWM inverters," *IEEE Trans. Ind. Appl.*, vol. IA-21, no. 4, pp. 562–570, Jun. 1985.

[32] A. B. Plunkett, "A current-controlled PWM transistor inverter drive," in *IEEE/IAS Annu. Meeting Conf. Record*, 1979, pp. 789–792.

[33] J. W. Nilsson, *Electric Circuits*. Reading, MA: Addison-Wesley, 1993.

T. A. Parlikar (S'98) received the B.S. degree in engineering and the B.A. degree in mathematics from Swarthmore College, Swarthmore, PA, in 2001. He received the S.M. degree from the Massachusetts Institute of Technology, Cambridge, in 2003. He is currently working toward the Ph.D. degree in the Laboratory for Electronic and Electromagnetic Systems at the Massachusetts Institute of Technology, Cambridge.

His research interests include dynamic systems modeling, estimation, and control, and its applications in fields such as power electronics, automotive systems, and biological systems.

Mr. Parlikar is a member of Sigma Xi, Tau Beta Pi, and Phi Beta Kappa. At Swarthmore he was awarded the Thomas McCabe Award given to the most outstanding engineering student in the senior class, and the Heinrich Brinkmann mathematics prize for the best undergraduate mathematics paper.

W. S. Chang (S'96–M'03) was born in Seoul, Korea. He received the B.S. and M.S. degrees in electrical engineering from Seoul National University in 1988 and 1990, respectively, and the S.M. degree in mechanical engineering and the Ph.D. degree in electrical engineering and computer science from the Massachusetts Institute of Technology, Cambridge, in 1999 and 2003, respectively.

From 1990 to 1996, he performed control application projects for consumer electronics and computer peripherals at Daewoo Electronics, Seoul, Korea. Since 2003, he has led advanced control projects for semiconductor equipment at Varian Semiconductor, Gloucester, MA. His main interests are in the area of design, analysis, mathematical modeling, simulation, and control of complex dynamic systems with a variety of applications, including robotic systems for semiconductor equipment, automotive electrical/electronic components and systems, consumer electronics, and computer peripherals.

Y. H. Qiu (S'02) received the B.S.E.E. and M.S.E.E. degrees from HuaZhong University of Science and Technology (HUST), China, in 1997 and 2000, respectively.

She joined the R&D center of Avansys Power Company Limited (China division of Emerson Network Power) as an Application Engineer in 2000. Since 2002, she has been with the Laboratory of Electromagnetic and Electronic Systems of Massachusetts Institute of Technology, Cambridge, where she is presently working toward the Ph.D. degree. Her research interests include motor control and power electronics.

Ms. Qiu was awarded the Siemens Fellowship for her outstanding work as a graduate student, and the GuangHua Prize given to the most outstanding students in her undergraduate class.

M. D. Seeman (S'02) received the S.B. degree in electrical engineering and physics from the Massachusetts Institute of Technology, Cambridge, in 2004. He is now working toward the M.S. and Ph.D. degrees at the University of California, Berkeley.

D. J. Perreault (S'91–M'97) received the B.S. degree from Boston University, Boston, MA, in 1989, and the S.M. and Ph.D. degrees from the Massachusetts Institute of Technology (MIT), Cambridge, in 1991 and 1997, respectively.

In 1997, he joined the MIT Laboratory for Electromagnetic and Electronic Systems as a Postdoctoral Associate, and became a Research Scientist in the laboratory in 1999. In July 2001, he joined the MIT Department of Electrical Engineering and Computer Science, where he is presently the Emanuel E. Landsman Associate Professor of Electrical Engineering and Computer Science. His research interests include design, manufacturing, and control techniques for power electronic systems and components, and their use in a wide range of applications.

Dr. Perreault received the Richard M. Bass Outstanding Young Power Electronics Engineer Award from the IEEE Power Electronics Society, an ONR Young Investigator Award, the SAE Ralph R. Teetor Educational Award, and has received two IEEE prize paper awards. He is a member of Tau Beta Pi and Sigma Xi.

J. G. Kassakian (S'65–M'73–SM'80–F'89) received the undergraduate and graduate degrees from Massachusetts Institute of Technology (MIT), and prior to joining the MIT faculty, served a tour of duty in the U.S. Navy.

He is Director of the MIT Laboratory for Electromagnetic and Electronic Systems, Cambridge.

Dr. Kassakian is the Founding President of the IEEE Power Electronics Society, and is the recipient of the IEEE Centennial Medal, the IEEE William E. Newell Award, the IEEE Power Electronics Society's Distinguished Service Award, and the IEEE Millennium Medal. He is a member of the National Academy of Engineering. He has published extensively in the areas of power electronics, education, and automotive electrical systems, and is a co author of the textbook *Principles of Power Electronics*.

T. A. Keim (M'90) received the Doctor of Science degree from the Massachusetts Institute of Technology (MIT), Cambridge.

Following graduation, he remained at MIT for several years as a member of the sponsored research staff, working on superconducting electric machines. He then worked for over a decade with General Electric Corporate Research and Development, where he contributed to and led work on superconducting electric machines and on superconducting electromagnets for medical nuclear magnetic resonance imaging. In his next position, he served for nearly a decade at Kaman Electromagnetics as a corporate officer and chief engineer. In this position, he led engineering of multiple high-performance electromechanical and power electronics systems, for applications ranging from military propulsion systems and launchers to traction systems for public transit to oil drilling machinery. Since 1998, Dr. Keim has again been at MIT, where he is a Principal Research Engineer and serves as the Director of the MIT/Industry Consortium on Advanced Automotive Electrical/Electronic Components and Systems. In this capacity, he conducts and directs research into the future of automotive electric power systems. He has more that 45 publications and 11 patents.